IOSR Journal of Applied Physics (IOSR-JAP)
e-ISSN: 2278-4861.Volume 14, Issue 2 Ser. II (Mar. – Apr. 2022), PP 01-10
www.iosrjournals.org

Uranium fingerprint for some sedimentary rock samples, Southwestern Sinai, Egypt

Shaimaa E. Abu Hassan[a], Eman M. Ibrahim[b], Ibrahim E. El Aassy[b] and Thanaa M. Abd El Maksoud[a]

[a]*Faculty of Women for Art, Science and Education, Ain Shams University, Cairo, Egypt*
[b]*Nuclear Materials Authority (NMA), P.O. Box 530, El-Maadi, Cairo, Egypt*

Abstract
One of the national nuclear security regimes in Egypt is to develop a national database for all the nuclear and radioactive sources used in its premises. This database should contain all the information regarding nuclear material such as chemical composition, physical form and activity concentration. In this work, ten rock samples collected from Allouga Quarry face have been used to determine the uranium fingerprint of these samples through the calculation of different activity ratios, uranium age dating and lead concentration. High purity germanium detector (HPGe) was used to estimate the specific activities and activity ratios of different radionuclides in the assayed samples. The specific activity ranges of ^{238}U, ^{232}Th, ^{235}U and ^{40}K are 495.74±20-13037.51±75.4, 10.21±0.67-79.87±1.4, 22.82±1.4-599.51±7.2 and 48.54±5.3-600.08±5 Bq/kg, respectively. The calculated abundance of ^{235}U for all studied samples varies from 0.70 to o.71 which is approximately natural value (0.72). Theil diagram clearly shows that uranium accumulation and leaching happened in the investigated Quarry Face, as evidenced by the samples located in forbidden zone. The $^{230}Th/^{232}Th$ activity ratios range between 8.76 and 112.85 for samples which are higher than 20 except one sample. So, after subtraction the detrital ^{230}Th, the corrected ages for uranium mineralization vary from 32.82 to 82.81 ky. Lead concentrations in variegated shale samples were higher than that for black shale and dolostone samples, according to chemical analyses.

Keywords: *Uranium Fingerprint, Allouga Quarry, Southwestern Sinai, Age Dating*

Date of Submission: 04-04-2022 Date of Acceptance: 19-04-2022

I. Introduction

The needs to have a national database for all radioactive materials become one of the important elements to enhance the nuclear security regime in the country. This database should include all the information related to radioactive material such as chemical composition, physical characteristics, isotopic ratio, concentration and any other associated information to use as fingerprint of these materials. Natural uranium contains three main isotopes ^{238}U, ^{235}U and ^{234}U with relative abundance 99.2, 0.72 and 0.0056 %, respectively [1]. The isotopic composition of uranium for radioactive material can reveal information about the material's history and is an indication of the material's intended use. To obtain fingerprint for nuclear material, it must be examined using various techniques. Many different physical and chemical techniques are used to analyses the concentrations of important radionuclides, trace elements content, the microstructure and the elapsed time since the last material was purified (radiological age). A set of these characteristics are called signatures which are used to develop a national database for all the radioactive samples, to provide control, protection and accounting to identify the origin using different physical and chemical techniques [2].

Uranium age dating in rock sample is used as fingerprint of the radioactive ore material. There are several traditional methods used to determine it, such as measuring the activity ratio of $^{214}Bi/^{234}U$ by high resolution gamma-spectrometry (Uranium age dating) [3], and another method is uranium thorium dating where the radioactive half-lives of the two alpha emitters ^{238}U and ^{230}Th was used [4]. This method can only be applied to samples which initially had no detrital ^{230}Th content [5].

For uranium ore deposits, the isotopic composition of lead was used as a signature for radioactive material. Physical and chemical fractionation processes are not effect on it, but depends on the age, the uranium and thorium content in the source rock, so it was changed with time as radiogenic lead is constantly produced. So lead from each uranium ore body carries a specific isotopic signature which is fixed at the time of its formation [6].

One of the most important signatures for radioactive materials was determination the concentration of the REEs which can be used as an evidence of uranium origin. Uranium occurs in large number of minerals.

These minerals are often associated with a variety of other metallic elements, which it is a specific for a particular deposit [7].

In this paper, the uranium fingerprint is established through the determination of specific activities and activity ratios of different radionuclides, uranium age dating and lead concentrations for the studied samples collected form Allouga Quarry face, southwestern Sinai, Egypt.

II. Uranium Fingerprint and Methodology

2.1. Isotopic analysis of ore samples

Isotopic composition of uranium could be used as a fingerprint for the rock samples. In our work a gamma-ray spectroscopy technique has been used to estimate the specific activities (Bq/kg) of the radionuclides found in the assayed samples using the following equation [8].

$$SA = \frac{CR}{\xi \times I_{\gamma} \times W \times G} \quad (1)$$

where CR is the net number of counts in a given peak area corrected from background peaks divided by counting time, ξ is the absolute efficiency of the used γ-ray spectrometer, I_{γ} is the abundance of gamma emissions per radioactive decay, W is the weight of measured sample (kg) and G is the geometry factor which is equal to unity when all measured samples were counted under the same conditions.

The measuring system's lowest limits of detection (LLD), which are necessary to evaluate the minimum detection level for suitable radionuclide determination using analytical technique, were determined using the following equation [9].

$$LLD = \frac{4.66 \times S_b}{\xi \times I_{\gamma}} \quad (2)$$

Where S_b is the estimated standard error of the net background count rate, ξ is the counting efficiency of the desired energy of the radionuclides, and I_{γ} is the abundance of gamma emissions per radioactive decay. The LLD of a measuring system determines how well it can operate without being influenced by the sample. High-resolution gamma spectrometry was used to assess the absolute determination of uranium abundance, which was characterised as [10].

$$^{235}U_{abu} = \frac{1}{1 + 3.479 \times 10^{-4} \times \left(\frac{^{234}U}{^{235}U}\right) + 6.43 \times \left(\frac{^{238}U}{^{235}U}\right)} \times 100 \quad (3)$$

Due to the low concentration of ^{234}U, equation 3 will be approximate to the following equation:

$$^{235}U_{abu} = \frac{1}{1 + 6.43 \times \left(\frac{^{238}U}{^{235}U}\right)} \times 100 \quad (4)$$

2.2. Uranium Age Dating

One of the advantages of using non-destructive assay (NDA) techniques for uranium age dating is suitability for any material and does not depend on physical form or geometrical shape. It uses intrinsic efficiency calibration to measure the daughter/parent activity ratio using high-resolution gamma spectrometry. This method does not necessitate the use of any known-age reference materials. To calculate uranium dating, use the equation below [11].

$$\left(\frac{^{230}Th}{^{234}U}\right) = \left(\frac{^{238}U}{^{234}U}\right) \times \left(1 - e^{-\lambda_{230} t}\right) + \left(\frac{\lambda_{230}}{\lambda_{230} - \lambda_{234}}\right) \times \left(1 - \frac{^{238}U}{^{234}U}\right) \times \left(1 - e^{-(\lambda_{230} - \lambda_{234})t}\right) \quad (5)$$

where t is the age of the sample, ($^{230}Th/^{234}U$) and ($^{238}U/^{234}U$) are the measured activity ratios, and λ_{230} and λ_{234} are the decay constants of ^{230}Th and ^{234}U, respectively. This method can be applied to objects, which initially had no detrital ^{230}Th content. Any initial thorium can be derived from the presence of the cosmogonic isotope ^{232}Th. Detrital components are not present if the $^{230}Th/^{234}U$ activity ratio is larger than 20.

^{234}U has decayed to $^{230}Th^*$ (radiogenic) during ageing, and the activity of $^{230}Th^*$ is computed using equation 6 from the measured total $^{230}Th_{total}$ activity (= Th*(radiogenic) + Th (detrital)). With Th index or ^{232}Th activity

increasing, the difference between the uncorrected ^{230}Th/U age determined from total $^{230}Th_{total}$ activity and the detritus-corrected ^{230}Th*/U age derived from [^{230}Th*] grows, decreasing the age.

$$\left[{}^{230}Th_{\,total}\right] = \left[{}^{230}Th^{*}\right] + \left[\frac{{}^{230}Th}{{}^{232}Th}\right].\left[{}^{232}Th\right] = \left[{}^{230}Th^{*}\right] + f.\left[{}^{232}Th\right] \qquad (6)$$

In the plot of ^{230}Th/^{232}Th activity ratio versus ^{234}U/^{232}Th activity ratio, the slope of the straight mixing line (Isochron) equals the actual ^{230}Th*/^{234}U activity ratio which is the important parameter for calculating ^{230}Th*/U ages. The present [^{230}Th/^{232}Th] activity ratio or the present thorium index f is obtained by intersecting the isochron on the Y axis [12].

2.3. Concentration of Pb

Lead has four naturally occurring isotopes; ^{206}Pb, ^{207}Pb and ^{208}Pb which are stable isotopes with relative abundance 24.1%, 22.1% and 52.4%, respectively [13] and ^{204}Pb is radioactive isotope with abundance 1.4% and life time $1.4x10^{17}$ year. ^{206}Pb, ^{207}Pb and ^{208}Pb are radiogenic daughters of radioactive parent isotopes ^{238}U, ^{235}U and ^{232}Th, respectively. Due to the extremely long half-life of the parent isotopes, the isotope composition of lead varies greatly from region to another so it can be used as one of the parameters to distinguish between materials of different origins. The Pb isotopic composition allows the characterization and identification of various lead sources in natural systems. The isotope ratios may be useful as a fingerprint of the element source [14].

By using inductive coupled plasma spectroscopy Pb concentration was measured in ppm. To evaluated lead isotopes concentration we can use the following equation:

$$^{x}Pb\ \% = (^{x}Pb/Pb) \times 100 \qquad (7)$$

III. Geologic Setting and Sampling

Ten rock samples were collected from Quarry face (6 samples) and north Quarry face (4 samples) of Gabal Allouga, Southwestern Sinai, Egypt, which were from different types of sedimentary rocks and different radioactive grades. Figure 1 shows the geologic map and localities of these samples. Table 1 illustrates the characteristic features of the assayed samples.

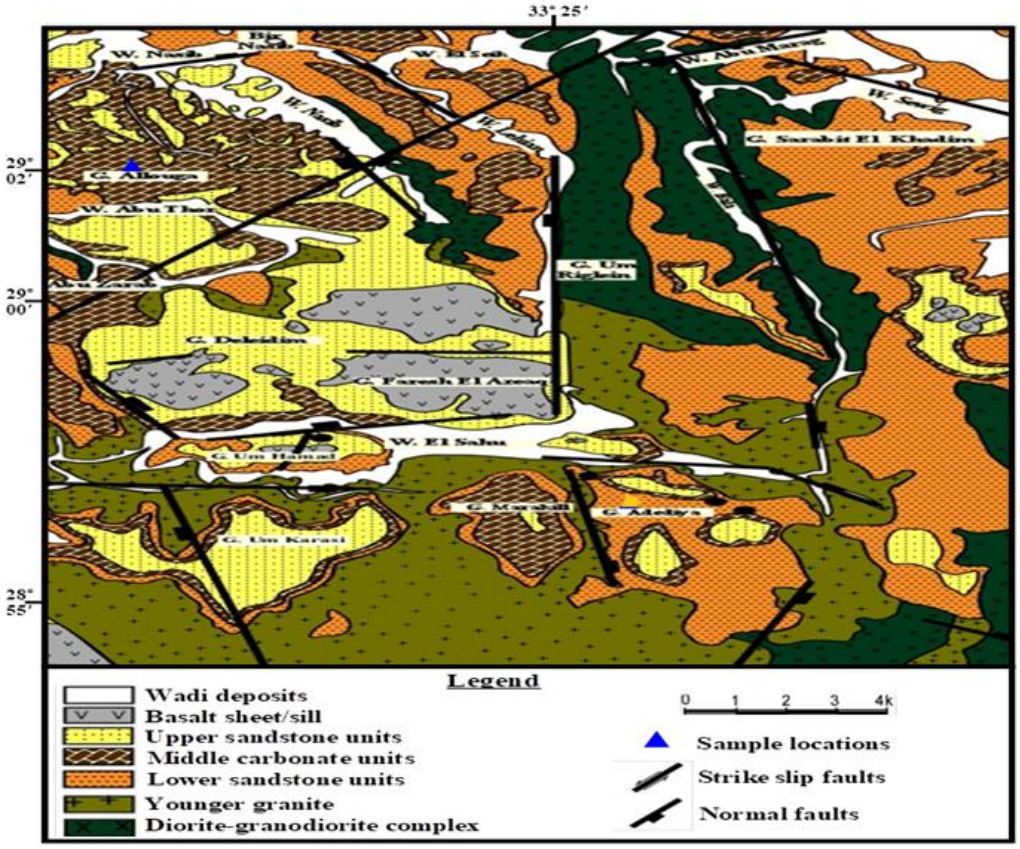

Fig. 1: Geologic map of the studied area with the localities of the collected samples.

Table 1 Description of the collected samples.

Locality	Samples No.	Description
Allouga Quarry Face	MR.1	• Black shale, fissile, slightly compact, representing the western side and one meter overlying the base of the face.
	MR.2	• Black shale as sample MR.1, four meters to the east of MR.1.
	MR.3	• Black shale as sample MR.1, four meters to the east of MR.2.
	MR.4	• Compact dolostone, grey to black, medium-hard to hard with green Cu mineralization, it is one-meter overlying sample MR.3.
	MR.5	• Compact dolostone as sample MR.4, it is one-meter overlying sample MR.2 and four meters west sample MR.4.
	MR.6	• Compact dolostone as sample MR.4 and located four meters to the west of sample MR.5 and one-meter overlying sample MR.1
North Quarry Face	B.1	• Variegated shale, brown, yellow and reddish, fissile, soft to medium-hard.
		• Variegated shale, 2 m north of the previous sample, highly ferruginous.
	B.2	• Variegated shale, 3 m to the north of sample B.2.
	B.3	• Variegated shale, yellowish-brown with yellow secondary uranium mineral as encrustation, 2 m to the north of sample B.3.
	B.4	

IV. Analytical Method

4.1. High purity germanium detector (HPGe)

The studied rock samples were crushed, sieved and packed in a polyethylene plastic Marinelli beaker of constant volume (200 ml) after that plastic Marinelli beakers were sealed with a PVC tape, and stored for one month before counting to allow secular equilibrium to be attained between Rn-222 and its parent Ra-226 in uranium chain [15]. The counting time for all samples varied between 20 and 25 h.

The isotopic composition analysis of samples was carried out using closed-end coaxial (GEM-502 10-P, Ortec) gamma-ray detector (p-type) made of high purity germanium (HPGe) which has relative efficiency 50% of the 3″x3″ NaI(Tl) crystal efficiency.

The detector is connected to conventional electronics through a PC computer's multichannel analyzer card (MCA). The efficiency calibration was carried out utilizing three standard reference materials for U, Th, and K activity measurements provided from the International Atomic Energy Agency (RGU-1, RGTh-1 and RGK-1, respectively) [16].

Uranium- 238 activity was determined indirectly from the gamma rays emitted by its daughter product (^{234m}Pa) whose activity was determined from the 1001 keV photo peak. The ^{234}U activity was determined directly from the gamma rays emitted from this nuclide at energy 120.9 keV. For the measurement of the ^{230}Th activity, the γ-ray emission at 67.7 keV is used. The specific activity of ^{226}Ra was measured using the 186.1 keV from its own gamma ray (after the subtraction of the 185.7 keV of ^{235}U). The specific activity of ^{214}Pb was measured using the 241.9, 295.2 keV and 351.9 keV while the specific activity of ^{214}Bi and ^{210}Pb were measured using 609.3 and 46.5 keV, respectively. The uranium-235 activity was determined directly by its gamma-ray peaks; 143.8, 163.4, 185.7 and 205.3 keV. The specific activity of ^{232}Th was measured using 911.2 keV from ^{228}Ac and 2614.4 keV from ^{208}Tl. The signature gamma-ray energy peak from ^{40}K at 1460.8 keV was observed in all samples as shown in Figure 2.

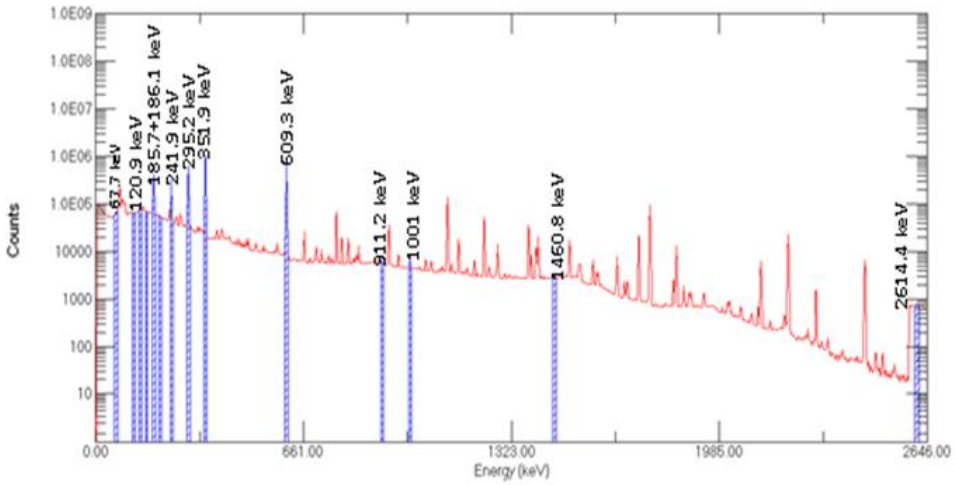

Fig. 2: Gamma ray spectrum of the studied sample (MR.4).

4.2. Inductive coupled plasma- optical emission spectrometer (ICP-OES)

Geological samples were digested using 5 ml HNO_3, 3 ml $HClO_4$ and 2 ml HF. The digestion process was performed in a microwave (MLS.1200 MEGA milestone. Italy). The used digestion program was at time 2 min (power was 250 watt), at time 5 min (power was 400 watt) finally at time 5 min (power was 500 watt). The digested samples were diluted with double deionized water 18 MΩ.

After digestion process, the geological samples diluted by double deionized water 18 mega ohm and then analyzed using ICP-OES. Prodigy axial high dispersion inductively coupled plasma- optical emission spectrometer (ICP-OES) was used in determination of elemental analysis in geological samples. The experimental conditions are "RF frequency 40 MHz, RF power 1.3 K watt, coolant gas flow rate 18 L/min, auxiliary rate flow 0.3 L/min, carrier gas pressure 34 psi, integration time 4 sec and sample intake rate 1.0 mL/sec".

V. Results and Discussions

The LLD values of radionuclides are found to be 9.7, 1.3, 3.1 and 18.7 Bq/kg for ^{238}U, ^{235}U, ^{232}Th and ^{40}K, respectively. The activity concentrations of ^{238}U, ^{235}U, ^{234}U, ^{230}Th, ^{226}Ra, ^{214}Pb, ^{214}Bi, ^{210}Pb, ^{232}Th and ^{40}K and their isotopic ratios are shown in Table 2, while $^{230}Th/^{234}U$, $^{234}U/^{238}U$ activity ratios and calculated ages are summarized in Table 3. The ISOPLOT program was used to calculate ages and errors [17].

The activity concentrations of ^{238}U for the analyzed samples vary from 495.74 to 13037.51 Bq/kg in black shale, from 2014.07 to 5316.73 Bq/kg in dolostone and from 3793.86 to 11889.56 Bq/kg in variegated shale, while ^{235}U activity concentrations vary from 22.82 Bq/kg to 599.51 Bq/kg in black shale, from 93 to 244.61 Bq/kg in dolostone and from 174.84 to 547.76 Bq/kg in variegated shale.

^{232}Th activity concentrations vary from 16.16 to 33.16 Bq/kg in black shale, from 10.21 to 15.39 Bq/kg in dolostone and from 58.14 to 79.87 Bq/kg in variegated shale, while ^{40}K activity concentrations vary from 48.54 to 314.31 Bq/kg in black shale, from 65.60 to 71.83 Bq/kg in dolostone and from 315.28 to 600.08 Bq/kg in variegated shale.

The results show that the rock samples have substantial activity levels of ^{238}U and its progenies. However, ^{232}Th was found in trace amounts, and its contribution to natural radioactivity from ore matrix is low, as seen in Figure 3.

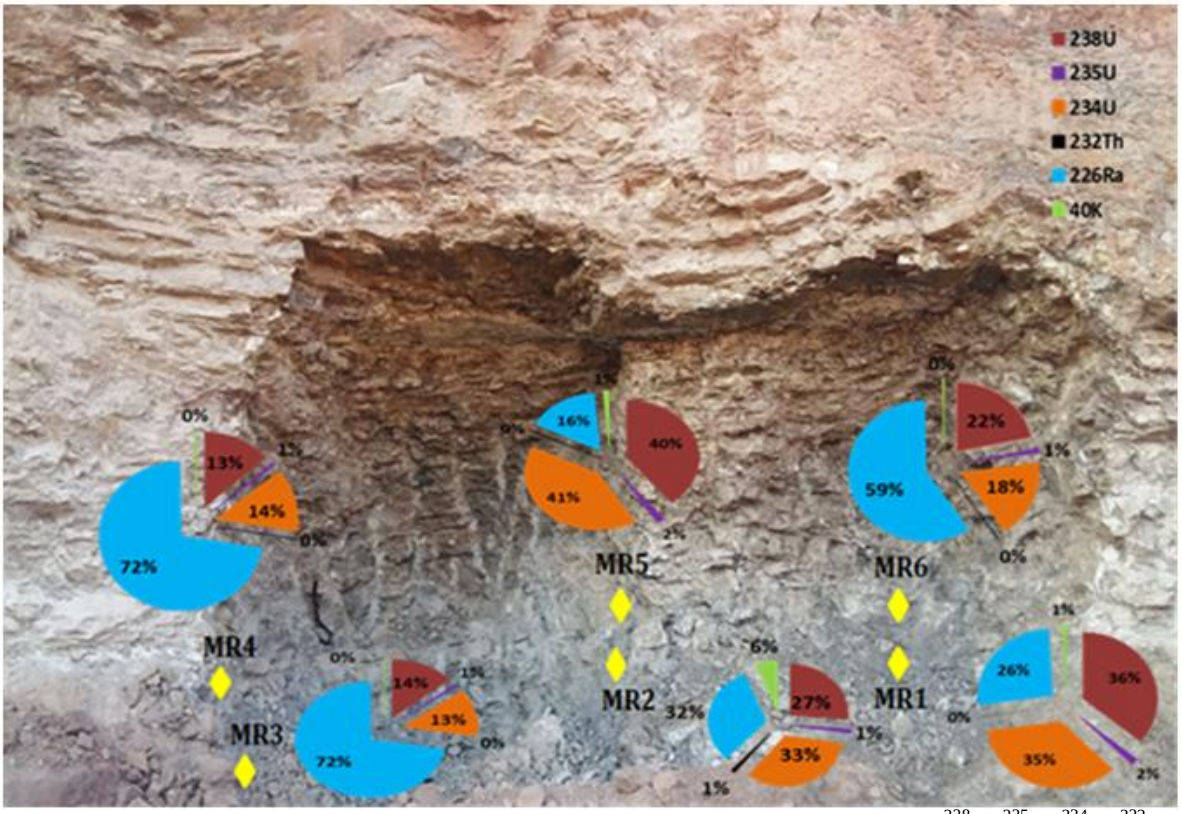

Fig. 3: Southern Face of Allouga Quarry showing activity concentration contributions of ^{238}U, ^{235}U, ^{234}U, ^{232}Th, ^{226}Ra and ^{40}K for (MR) samples.

5.1. Activity Ratios

After 1.7 Ma, the radionuclides ^{238}U, ^{234}U and ^{230}Th reach radioactive equilibrium in closed geologic systems [18], with activity ratios $^{230}Th/^{234}U$, $^{230}Th/^{238}U$ and $^{234}U/^{238}U$ are all equal unity. The differing physicochemical conditions impacting ^{238}U and ^{234}U will result in their fractionation if the systems are subject to weathering and groundwater circulation, and thus the corresponding daughter/parent radionuclide activity ratios in the decay series will not equal unity.

Uranium isotope variation is caused by the selective leaching of ^{234}U and the direct α-recoil transfer of a ^{234}U precursor (^{234}Th). A $^{234}U/^{238}U$ activity ratio less than or greater than 1 indicates that a uranium isotope has migrated within the rock in the last 1 to 2 million years; the time required for ^{234}U to reach secular equilibrium [19]. Because of changes in radionuclide mobility during weathering processes, weathered rocks diverge from secular equilibrium in general. This relative mobility is believed to be $^{234}U>^{238}U>^{230}Th$, so the weathered rocks are estimated to have $^{234}U/^{238}U<1$ and $^{230}Th/^{238}U>1$.

The activity ratios of various radionuclides in different rock types (Table 2) show what occurred in these rocks. The $^{234}U/^{238}U$, $^{230}Th/^{238}U$, $^{230}Th/^{234}U$ and $^{226}Ra/^{238}U$ activity ratios for the examined samples show fractionation of uranium and thorium isotopes during chemical weathering.

The activity ratios of $^{238}U/^{235}U$ for all studied samples are ranging between 21.66 and 21.93, which reflect nearly the natural ratio (21.7) as shown in Figure 4a. Although considerable fluctuations in the $^{238}U/^{235}U$ ratio have only recently been discovered, significantly larger changes in the $^{234}U/^{235}U$ ratio have long been observed in terrestrial variations.

The higher mobility of ^{234}U compared to other uranium isotopes is due to its production from ^{238}U via α -decay and subsequent emplacement at crystal sites damaged by α -recoil. The preferential leaching of ^{234}U from these α-damaged crystal sites occurs as a result of aqueous weathering of materials containing uranium [20]. In contrast to the $^{238}U/^{235}U$ activity ratios, the $^{234}U/^{235}U$ activity ratios varied from 16.99 to 27.42, indicating uranium-234 leaching out in some samples and migrating in others due to alteration processes (Figure 4b).
The abundance of ^{235}U for all studied samples are vary from 0.70 to o.71 as shown in Table 2, which illustrated nearly no deviation from the natural value (0.72).

Table 2 Specific activities (Bq kg^{-1}) of different radionuclides and activity ratios for studied samples.

	Quarry Face						North Quarry Face			
	Black Shale			Dolostone			Variegated Shale			
	MR.1	MR.2	MR.3	MR.4	MR.5	MR.6	B.1	B.2	B.3	B.4
^{238}U	13037.51±75.4	495.74±20	5469.89±169	3412.95±110.9	2014.07±27.4	5316.73±61.8	5996.39±98.1	4240.31±78.2	3793.86±74.3	11889.56±132.5
^{234}U	12684.52±1496.8	625.92±124.56	5266.84±516.4	3463.62±388.3	2093.95±243.3	4366.97±582.4	4688.07±1523.8	3472.19±744.8	3350.74±433.1	9743.43±860
^{230}Th	3742.17±210.8	181.35±41.1	14987.47±338.9	8617.181±253.2	605.26±81.1	1266.91±116.44	5457.6±403.1	4617.84±254.8	4962.64±273	5119.04±360.3
^{226}Ra	9540.07±15.5	601.15±4	28744.84±165.8	18345.87±27.5	823.54±4	14474.1±24.9	12399.52±31.3	9069.09±18.8	10088.1±17	15117.94±29.1
^{214}Pb	5733.24±5.6	355.8±1.4	15048.22±9.5	9076.74±7.1	572.95±1.7	6808.65±6.4	8619.64±9.7	6416.33±5.8	7293.2±5	11216.08±9.5
^{214}Bi	5790.39±5.3	363.81±1.3	15279.59±8.9	9200.36±6.6	575.09±1.5	6923.78±6	8695.86±8.9	6556.62±5.6	7389.41±4.7	11387.57±8.9
^{210}Pb	3836.1±615	395.1±110.62	3084.47±834.67	2789.28±515.11	184.06±69.26	2714.72±573.79	4517.19±847.48	3374.16±532.55	3483.04±446.76	3703.13±1371.2
^{235}U	599.51±7.2	22.82±1.4	249.37±5.2	157.12±5.8	93±2.6	244.61±4.6	275.94±8.1	195.11±5.8	174.84±3.6	547.76±8.7
^{232}Th	33.16±2.4	20.69±0.6	16.16±3.3	11.11±2.1	10.21±0.67	15.39±2.1	66.3±2.6	67.25±1.8	79.87±1.4	58.14±2.7
^{40}K	314.31±4.7	114.97±2	48.54±5.3	71.83±5.1	65.65±1.5	65.6±5	434.74±10.3	315.28±5.3	600.08±5	432.44±7.9
$^{238}U/^{235}U$	21.75±0.39	21.72±2.21	21.93±1.14	21.72±1.51	21.66±0.9	21.74±0.66	21.73±0.99	21.73±1.05	21.69±0.87	21.71±0.59
$^{234}U/^{235}U$	21.16±2.75	27.42±7.14	21.12±2.51	22.04±3.29	22.52±3.25	17.85±2.72	16.99±6.02	17.79±4.35	19.16±2.87	17.79±1.85
$^{234}U/^{238}U$	0.97±0.12	1.26±0.30	0.96±0.12	1.01±0.15	1.04±0.13	0.82±0.12	0.78±0.27	0.82±0.19	0.88±0.13	0.82±0.08
$^{230}Th/^{238}U$	0.29±0.02	0.37±0.1	2.74±0.15	2.52±0.16	0.30±0.04	0.24±0.02	0.91±0.08	1.09±0.08	1.31±0.1	0.43±0.01
$^{230}Th/^{234}U$	0.29±0.05	0.29±0.12	2.85±0.34	2.49±0.35	0.29±0.07	0.29±0.07	1.164±0.46	1.33±0.36	1.48±0.27	0.53±0.08
$^{230}Th/^{232}Th$	112.85±14.52	8.77±2.24	927.44±210.36	775.62±169.39	59.28±11.83	82.32±18.79	82.32±9.3	68.67±5.63	62.1339841±4.51	88.05±10.29
$^{226}Ra/^{238}U$	0.73±0.01	1.21±0.06	5.26±0.19	5.38±0.18	0.41 ±0.01	2.72±0.03	2.07±0.04	2.14±0.04	2.66±0.06	1.27±0.02
$^{226}Ra/^{230}Th$	2.55±0.15	3.31±0.77	1.92±0.05	2.13±0.07	1.36±0.19	11.42±1.07	2.27±0.17	1.96±0.11	2.032±0.12	2.95±0.21
Abundance of ^{235}U	0.71	0.71	0.70	0.71	0.71	0.71	0.71	0.71	0.71	0.71

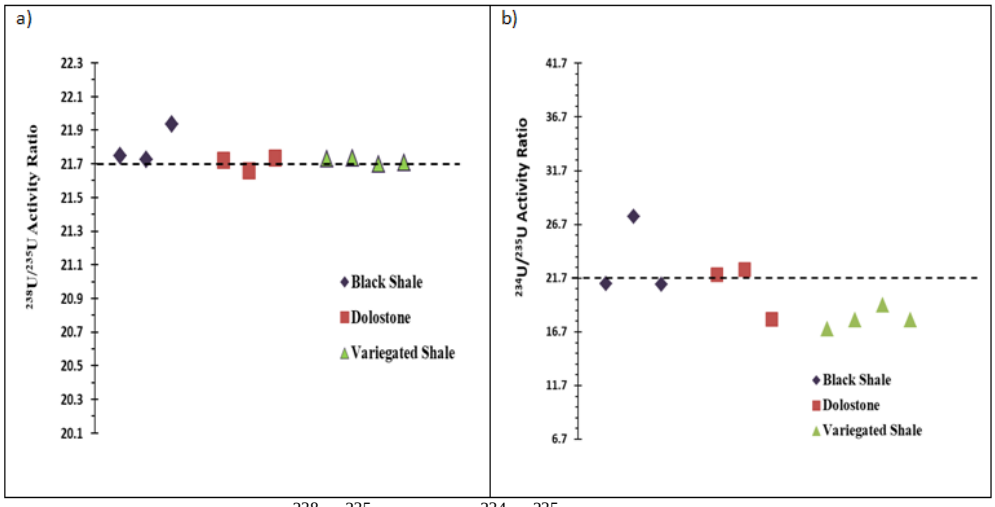

Fig. 4: Variations of; (a) $^{238}U/^{235}U$ and (b) $^{234}U/^{235}U$ activity ratios in the studied samples.

The $^{234}U/^{238}U$ activity ratio ranges between 0.96 and 1.26 with an average of 1.11 for black shale samples. For dolostone samples, the $^{234}U/^{238}U$ activity ratio ranges between 0.82 and 1.04 with an average of 0.93, while it ranges between 0.78 and 0.88 with an average of 0.83 for variegated shale samples.

Because of the alpha-recoil process and preferential leaching of ^{234}U relative to ^{238}U, the activity ratios of $^{234}U/^{238}U$ can be used as indicators for processes affected the (MR) samples which represent the face of the Quarry. Most samples (MR) show equilibrium between ^{234}U and ^{238}U except two samples (MR.2 and MR.6) which indicate migration of uranium in this location.

$^{234}U/^{238}U \leq 1$ and $^{230}Th/^{234}U > 1$ are common characteristics of uranium removal from rocks [21] which are similar to the studied samples (MR.3, MR.4, B.1, B.2 and B.3) as shown in Figure 5a. Reason for these ratios is that groundwater leaches ^{234}U preferentially to ^{238}U and removes both uranium isotopes in comparison to ^{230}Th; nevertheless, the activity ratios later changed to $^{234}U/^{238}U < 1$ and $^{230}Th/^{234}U < 1$ like the samples (MR.1, MR.6 and B.4). This is due to the late adsorption of uranium from water with $^{234}U/^{238}U < 1$ by the rock matrix.

Radium is easily mobilized under reducing conditions but readily adsorbed onto minerals formed in oxidized zones, such as iron hydroxides, whereas U is immobile in a reducing environment and only becomes soluble under oxidizing conditions; the $^{226}Ra/^{238}U$ activity ratio is also a good indicator for alteration processes [22] and migration of either ^{238}U or ^{226}Ra depending on the pH prevailed. The activity ratios of $^{226}Ra/^{238}U$ are greater than 1 for most studied samples with the exception of (MR.1 and MR.5) as shown in Figure 5b which indicate that there are disequilibrium between ^{238}U and ^{226}Ra and reflect migration in of ^{226}Ra resulting from recoil-implanted ^{226}Ra atoms from decay of ^{230}Th atoms and Ra readily adsorbed onto minerals, while (MR.1 and MR.5) samples have reverse case.

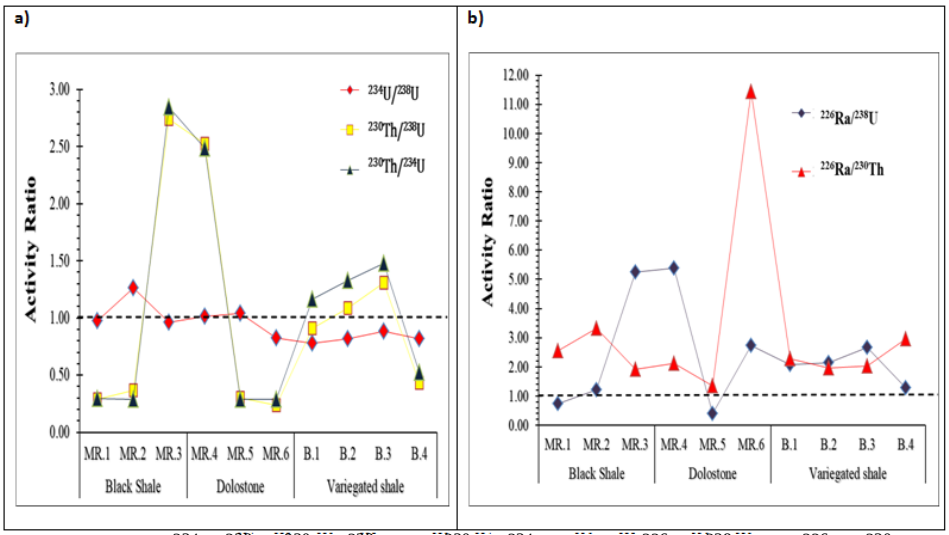

Fig. 5: Variations of the (a) $^{234}U/^{238}U$, $^{230}Th/^{238}U$ and $^{230}Th/^{234}U$ and (b) $^{226}Ra/^{238}U$ and $^{226}Ra/^{230}Th$ activity ratios in the studied samples.

5.2. Theil Diagram

Figure 6 illustrates a plot of $^{234}U/^{238}U$ versus $^{230}Th/^{238}U$, the return-to-equilibrium pathways of the solid phases appear for two states: accumulation of U ($^{230}Th/^{238}U$ decrease) and leaching of U ($^{230}Th/^{238}U$ increase) [23]. Continuous and contrasting U mobilization processes can explain the occurrence of data points in forbidden zones [24].

According to judging standards, the activity ratios between 0.90 and 1.10 are referred as secular equilibrium for the samples [25]. It is supported by the Thiel diagram (Figure 6) in which the samples that plot into the boxed-in area are considered near or at secular radioactive equilibrium. All cases of U leaching are characterized by ($^{234}U/^{238}U$ activity ratio < 1) and all cases of U accumulation are distinguished by the ($^{234}U/^{238}U$ activity ratio > 1) [23]. As shown in Figure 6, uranium accumulation occurs in (MR.2; black shale) while uranium leaching occurs in (B.1, B.2 and B.3; variegated shale) which are confirmed by the samples located in forbidden zone (MR.6; dolostone and B.4; variegated shale).

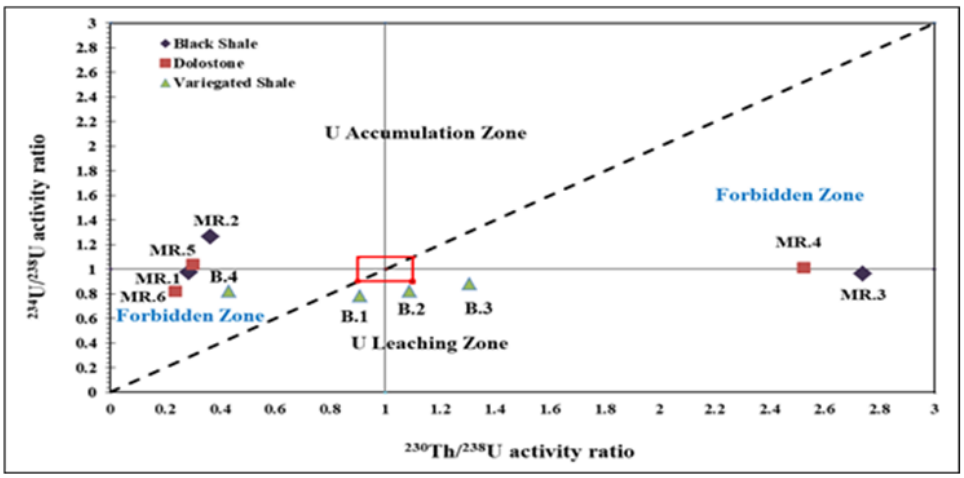

Fig. 6: Thiel diagram showing the evolution of $^{234}U/^{238}U$ versus $^{230}Th/^{238}U$ activity ratios.

5.3. Uranium Age Dating

The calculated uranium deposition ages on the studied samples are shown in Table 3. The presence of radioactive disequilibria among radionuclides in the decay series indicates recent fractionation events, which are frequently associated with the gain or loss of more mobile radionuclides [26].

According to Fontes et al. [27], changing redox conditions can cause uranium gain or loss in lacustrine samples. The calculated U-series date is younger than the true age due to uranium gain, while the date is older due to uranium loss[28].

The understanding of the U-migration process is important for computing the uranium dating results [29]. Samples (MR.3; black shale), (MR.4; dolostone) and (B.1, B.2 and B.3; variegated shale) show severe differential isotopic fractionation. These samples have an excess of $^{230}Th/^{238}U$ and the activity ratio $^{230}Th/^{234}U$ is more than 1 and therefore being undated because, in this case, the activity of the daughter exceeds the secular equilibrium with its parent.

The $^{230}Th/^{232}Th$ activity ratios range between 8.77 and 927.44 for all samples which are greater than 20 and indicate the absence of detrital components except (MR.2).

The global detrital correction factor $^{230}Th/^{232}Th$ is calculated by plotting the $^{230}Th/^{232}Th$ activity ratios against the $^{234}U/^{232}Th$ activity ratios. This factor is then used to correct each sample separately. The isochron-corrected ages of five samples were corrected with a $^{230}Th/^{232}Th$ ratio of 0.6088 as shown in Figure 7. By using equation 6 the actual radiogenic ^{230}Th and age of studied samples are calculated.

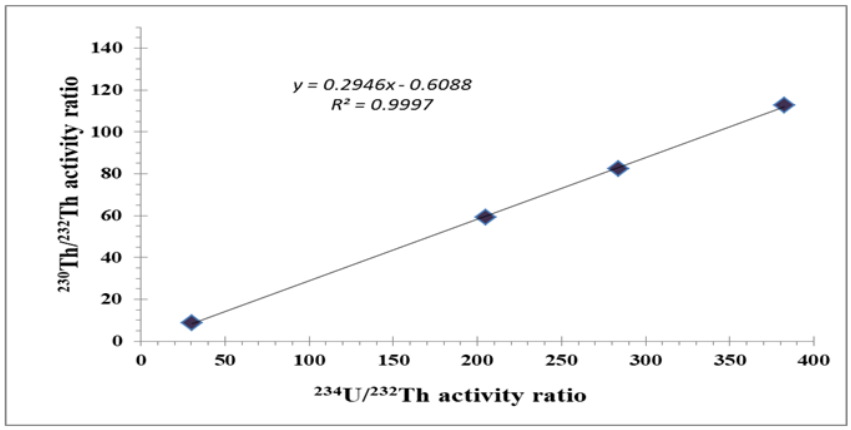

Fig. 7: $^{230}Th/^{232}Th$ vs $^{234}U/^{232}Th$ activity ratio isochron diagram.

As shown in Table 3, the ages of uranium depositions for black shale and dolostone samples are 38.08, 36.63, 37.01 and 37.76 ky, respectively, while for variegated shale sample is 84.06 ky. So, after subtraction the detrital ^{230}Th, the corrected ages for Quarry Face samples vary from 32.82 to 37.77 ky while for upper part (variegated shale) sample is 82.81 ky. The plot of the $^{238}U/^{234}U$ activity ratios versus the detritus-corrected $^{230}Th/^{234}U$ activity ratios is used to verify closed system conditions (Figure 8).

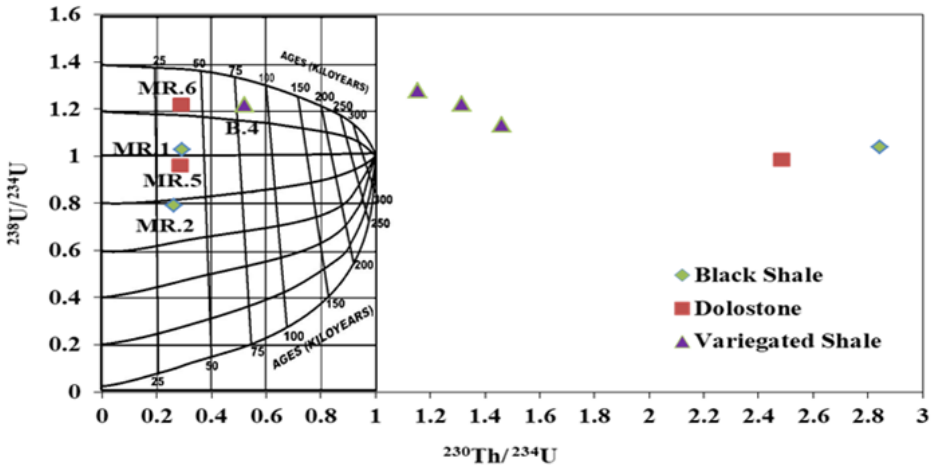

Fig. 8: Cross plot of isotopic ratios for studied sample.

Table 3 Specific activities of ^{238}U, ^{234}U and ^{230}Th, isotopic activity ratios and ages of uranium deposition for the studied samples.

Samples No.	^{238}U	^{234}U	^{230}Th	^{232}Th	$^{234}U/^{238}U$	$^{230}Th/^{234}U$	$^{230}Th/^{232}Th$	Age (ky)*		Age (ky)**	
MR.1	13037.51±75.4	12684.52±1496.8	3742.17±210.8	33.16±2.4	0.97±0.12	0.29±0.05	112.85±14.52	38.08	+2.83 -4.02	37.77	+2.85 -4.04
MR.2	495.74±20	625.92±124.56	181.35±41.1	20.69±0.6	0.79±0.19	0.29±0.12	8.76±2.24	36.63	+2.25 -5.35	32.82	+2.5 -5.88
MR.5	2014.07±27.4	2093.95±243.3	605.26±81.1	10.21±0.67	1.04±0.13	0.29±0.07	59.28±11.83	37.01	+2.69 -4.46	36.4	+2.74 -4.51
MR.6	5316.73±61.8	4366.97±582.4	1266.91±116.44	15.39±2.1	0.82±0.12	0.29±0.07	82.32±18.79	37.76	+2.77 -4.26	37.29	+2.80 -4.29
B.4	11889.56±132.5	9743.43±860	5119.04±360.3	58.14±2.7	0.82±0.08	0.53±0.08	88.05±10.29	84.06	+1.62 -2.23	82.81	+1.64 -2.25

*The uncorrected age for samples.
**The corrected age after subtraction detrital ^{230}Th for samples.

5.4. Concentration of Pb

Table 4 summarizes the results of the chemical analysis for the Pb in the studied rock samples and data measured by ICP-OES. It is observed that the total lead concentrations in variegated shale vary from 63.17 to 117.13 ppm which are higher than that for black shale and dolostone samples. This case is similar to the case of uranium concentrations which are high in variegated shale samples compared with dolostone samples. The concentrations of natural lead isotopes (^{204}Pb, ^{206}Pb, ^{207}Pb and ^{208}Pb) are calculated by using equation (7). The concentration of Pb isotopes reflect the variation of concentration of ^{238}U, ^{235}U and ^{232}Th (Tables 2 and 4)

Table 4 Lead concentrations (ppm) for the studied samples by using ICP-OES.

	Quarry Face						North Quarry Face			
	Black Shale			Dolostone			Variegated Shale			
	MR.1	MR.2	MR.3	MR.4	MR.5	MR.6	B.1	B.2	B.3	B.4
Pb	33.28	60.13	25.51	12.26	16.84	17.05	63.17	64.28	79.08	117.13
^{204}Pb	0.47	0.84	0.36	0.17	0.24	0.24	0.88	0.89	1.11	1.64
^{206}Pb	8.02	14.49	6.15	2.96	4.06	4.11	15.22	15.49	19.06	28.23
^{207}Pb	7.35	13.29	5.64	2.71	3.72	3.77	13.96	14.21	17.48	25.89
^{208}Pb	17.44	31.51	13.37	6.42	8.82	8.93	33.1	33.68	41.44	61.38

VI. Summary And Conclusion

For enhancing the nuclear security regime in any country, a national database for all radioactive materials becomes one of the important elements. This database is used as fingerprint of these materials. In our study, the fingerprint of uranium is determined for some rock samples which are collected from Allouga Quarry face, Southwestern Sinai, Egypt. This fingerprint is established through the determination of activity concentrations and activity ratios for different radionuclides, uranium age dating and lead concentration for the studied samples.

The activity concentrations of ^{238}U and its progenies are higher than that for ^{232}Th in all samples. Different activity ratios of the studied samples show fractionation of uranium and thorium isotopes during chemical weathering. Theil diagram showed that uranium was accumulating and leaching in some samples, which was corroborated by samples located in forbidden zone.

The ages of uranium depositions for black shale and dolostone samples are 38.08, 36.63, 37.01 and 37.76 ky, respectively, while for variegated shale sample is 84.06 ky. After subtraction the detrital ^{230}Th, the corrected ages for Quarry Face samples vary from 32.82 to 37.77 ky while for North Quarry Face sample is 82.81 ky.

According to chemical analysis, the lead concentration in variegated shale samples is higher than that for black shale and dolostone samples.

References

[1]. P. Vesterbacka, Academic Dissertation, Faculty of Science, University of Helsinki, STUK-A213, Helsinki, 92, (2005).
[2]. A.I. Apostol, A. Pantelica, I. Ortega-Feliu, N. Marginean, O. Sima, M. Straticiuc, M.C. Jimenez-Ramos and V. Fugaru, J. Radioanal. Nucl. Chem. **311**(2), 1339–46 (2017).
[3]. A.M. Gaffney, A. Hubert, W.S. Kinman, M. Magara, A. Okubo, F. Pointurier, K.C. Schorzman, R.E. Steiner and R.W. Williams, Nucl. Chem. **307**(3), 2055–60 (2016).
[4]. Y.H. Dawood, M.A. Aref, M.H. Mandurah, A. Hakami and M. Gameil, J. Asia. Ear. Sci. **77**, 151–62 (2013).
[5]. T. Huisheng and R.G. Bednarik, Archaeol. Anthropol. Sci. **13**(1) (2021).
[6]. A.M.D. Vecchia, P.C.H. Rodrigues, F.J. Rios and A.C.Q. Ladeira, J. Geol. **47**(1), 147–58 (2017).
[7]. J. Švedkauskaitė - LeGore, European Commission Joint Research Centre in Karlsruhe, Germany, 102 (2008).
[8]. M. Tzortzis, H. Tsertos, S. Christofides and G. Christodoulides, Radia. Measur. **37**(3), 221–29 (2003).
[9]. M.A. Imtiaz, A. Begum, A.S. Mollah and M.A. Zaman, Heal. Phys. **88**(2), 169–74 (2005).
[10]. B.V. Loat, L.T. Anh, N.C. Tam, P.D. Khue and B.M. Hue, VNU J. Sci.: Mathe.-Phys. **29**(2), 33–39 (2013).
[11]. A. Kaufman and W. Broecker, J. Geophy. Rese. **70**(16), 4039–54 (1965).
[12]. M.A. Geyh, Geochronom. **20**, 9–14 (2001).
[13]. J. Meija, T.B. Coplen, M. Berglund, W.A. Brand, P.D. Bièvre, M. Gröning, N.E. Holden, J. Irrgeher, R.D. Loss, T. Walczyk and T. Prohaska, Pur. Appl. Chem. **88**(3), 293–306 (2016).
[14]. J. Švedkauskaitė-LeGore, G. Rasmussen, S. Abousahl and P. Van Belle, J. Radioanal. Nucl. Chem. **278**(1), 201–9 (2008).
[15]. M. Tufail, Environ. Sci. Pollut. Rese. **19**, 3327–38 (2012).
[16]. A.O. Mustapha, J.P. Patel, I.V.S. Rathore, N.O. Hashim and D. Otwoma, Appl. Radia. Isot. **60**(1), 79–82 (2004).
[17]. R.K. Ludwig, ISOPLOT a plotting and regression program for radiogenic-isotope data, V. 2.57. U.S. Geol. Surv., Open File Rept. 40 (1992).
[18]. M. Gascoyne, N.H. Miller and L.A. Neymark, Appl. Geochem. **17**(6), 781–92 (2002).
[19]. M. Pekala, J.D. Kramers and H.N. Waber, Appl. Radia. Isot. **68**(6), 984–92 (2010).
[20]. G.A. Brennecka, L.E. Borg, I.D. Hutcheon, M.A. Sharp and A.D. Anbar, Ear. Planet. Sci. Lett. **291**(1–4), 228–33 (2010).
[21]. Y.H. Dawood, Appl. Radia. Isot. **55**(6), 881–87 (2001).
[22]. I.E. El Aassy, M.M. El Galy, A.A. Nada, M.G. El Feky, T.M. Abd El Maksoud, S.M. Talaat and E.M. Ibrahim, J. Radioanal. Nucl. Chem. **289**(1), 173–84 (2011).
[23]. K. Thiel, R. Vorwerk, R. Saager and H.D. Stupp, Ear. Planet. Sci. Lett. **65**(2), 249–62 (1983).
[24]. F. Chabaux, J. Riotte and O. Dequincey, Rev. Mineral. Geochem. **52**(1), 533–76 (2003).
[25]. M. Min, X. Peng, J. Wang and J.K. Osmond, Appl. Radia. Isot. **63**(1), 115–25 (2005).
[26]. M. Condomines, O. Loubeau and P. Patrier, Chem. Geol. **244**(1–2), 304–15 (2007).
[27]. J.C. Fontes, J.N. Andrews, C. Causse and E. Gibert, Radiocar. **34**(3), 602–10 (1992).
[28]. B.J. Szabo, C.V. Haynes and T.A. Maxwell, Palaeogeo. Palaeoclim. Palaeoecol. **113**(2–4), 227–42 (1995).
[29]. J.J. Simpson and R. Grün, Quat. Sci. Rev. **17**(11), 1009–22 (1998).